



The ultimate regime of convection over uneven plates

Robert Kaiser, Julien Salort, Philippe-Emmanuel Roche

► To cite this version:

Robert Kaiser, Julien Salort, Philippe-Emmanuel Roche. The ultimate regime of convection over uneven plates. Journal of Physics: Conference Series, 2011, 318, pp.052044. 10.1088/1742-6596/318/5/052044 . hal-00640532

HAL Id: hal-00640532

<https://hal.science/hal-00640532>

Submitted on 13 Nov 2011

HAL is a multi-disciplinary open access archive for the deposit and dissemination of scientific research documents, whether they are published or not. The documents may come from teaching and research institutions in France or abroad, or from public or private research centers.

L'archive ouverte pluridisciplinaire **HAL**, est destinée au dépôt et à la diffusion de documents scientifiques de niveau recherche, publiés ou non, émanant des établissements d'enseignement et de recherche français ou étrangers, des laboratoires publics ou privés.

The ultimate regime of convection over uneven plates

R. Kaiser¹, J. Salort, P.-E. Roche

Institut Néel, CNRS/UJF, BP 166, F-38042 Grenoble cedex 9, France

Abstract. A new regime of convection, with a unprecedented heat transfer efficiency ($Nu \sim Ra^{0.38}$) has been observed in Grenoble in 1996 and named the *Ultimate Regime*. Following the prediction of Kraichnan in 1962, this regime has been interpreted as the asymptotic regime of convection, expected in the limit of very high thermal forcing ($Ra \rightarrow \infty$). A systematic study of the experimental conditions for the triggering of the *Ultimate Regime* has been conducted over the last decade. It revealed that the transition threshold is dependent on an unknown fixed length scale of the convection cells, in addition to the expected dependence versus the cell height. The cell diameter is a good candidate for this unknown scale and the observed sensitivity to the sidewall conditions tends to support this view. In the present study, we test an alternative candidate length scale associated with flatness defects of the heating and cooling plates. This hypothesis was tested by measuring the heat transfer in an elongated cell (aspect ratio 0.23) before and after introducing a controlled alteration of its surface flatness. Four smooth depressions have been formed on each plate, and their depth is of the order of the thermal boundary thickness at transition. The measurements show that such defect has no significant influence on the transition to the *Ultimate Regime*.

1. Introduction

A common model system to investigate thermal convection is the Rayleigh-Bénard cell. Inside a RB-convection cell, flow is driven by temperature difference between the top and bottom plates. Such an experiment is parameterized by a few dimensionless numbers. The Rayleigh number $Ra = g\alpha\Delta h^3/\nu\kappa$ characterizes the temperature difference between the top and bottom plates $\Delta = T_{\text{bottom}} - T_{\text{top}}$. The Prandtl number $Pr = \nu/\kappa$ specifies the molecular transport properties of the investigated flow. While the aspect ratio $\Gamma = d/h$ describes the geometrical conditions of the cylindrical RB-cell. g is the gravity. ν and κ are the kinematic viscosity and thermal diffusivity. α is the thermal expansion coefficient. h and d are cell height and cell diameter. For given Ra , Pr and Γ , the system response can be characterized by the Nusselt number $Nu = \dot{Q}_{\text{convection}}/\dot{Q}_{\text{diffusion}}$, which is the convective heat transport normalized by the diffusive heat transport that would settle in the absence of convection.

Nearly fifteen years ago, a transition to an enhanced heat transfer, compared to the well established hard turbulence $Nu \sim Ra^{1/3}$ -scaling, was reported at high Ra (Chavanne *et al.*, 1997). This observation was interpreted as the asymptotic regime of convection, predicted by Kraichnan (1962) and named *Ultimate Regime*. Over the recent years, intensive experimental efforts were made to understand this *Ultimate Regime* (Roche *et al.* (2010) and reference within). These investigations have shown that for a fixed Pr the triggering of the *Ultimate Regime*

¹ present address: Ilmenau University of Technology, Institute of Thermo- and Fluidynamics, 98693 Ilmenau, Germany

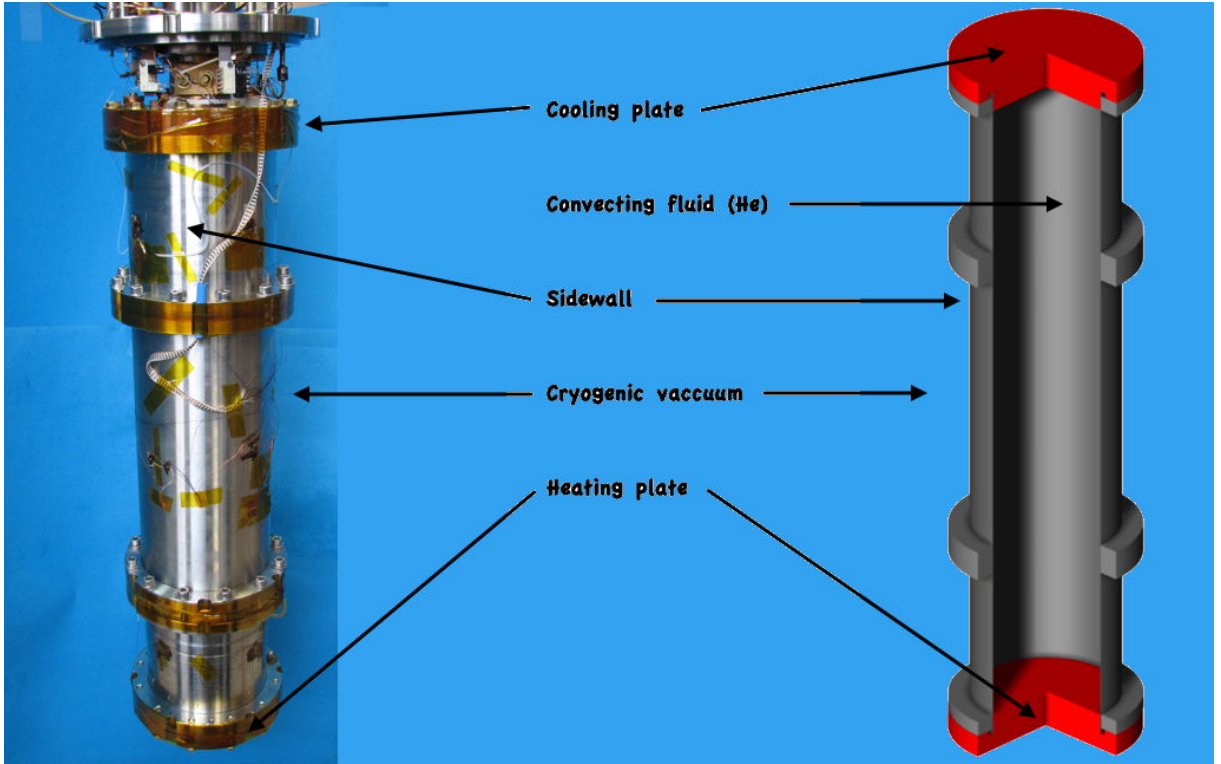


Figure 1. Photograph and sketch of the elongated Rayleigh-Bénard cell used in this study.

occurs at different Ra in cells of different heights but similar diameter. The transition Ra scales like $\sim \Gamma^{-3}$ for Γ of order 1, which suggests that a length scale common to all cells controls the transition (Roche *et al.*, 2010). The systematic experimental study which evidenced the existence of this length scale also showed that it cannot be associated with deviations from the Boussinesq approximation, from details on the sidewall nor with a Pr dependence (Roche *et al.*, 2010). The cryogenic environment and protocol of this previous study allowed to exclude length scales which would be related with residual heat leak (shown to be negligible regarding to cryogenic vacuum isolation of the suspended cell, and low black body radiation around 6 K), plate thermal response static/dynamic cut-off (due to high conductivity and low thermal inertia of cryogenic copper) or cell filling procedure (the cell is operated after being closed by a micro valve located close to the cell and isolated by a thermal siphon). Possible remaining fixed length scales are the cell diameter and length scales related with a residual defect in the flatness of the plates. Such defect on flatness could possibly favour the transition if the thermal boundary layer in the vicinity of the plates is thin enough to feel these defects.

In the present study, we compare the heat transfer in an elongated cylindrical cell ($\Gamma = 0.23$, figure 1) before and after alteration of the top and bottom thermal plates. For reference, we point that recent numerical simulations have been done in this elongated geometry (Stevens *et al.*, 2011).

2. Experiment description

The diameter of the cells is 10 cm with a height of 43 cm. The plates are made of annealed OFHC copper and are 2.5 cm thick. The conductivity of the plates is 1090 W/mK at 4.2 K and was measured *in situ*. As a first experiment we measured the heat transfer through a cell with very smooth and even plates. First measurements have already been published in (Roche *et al.*,

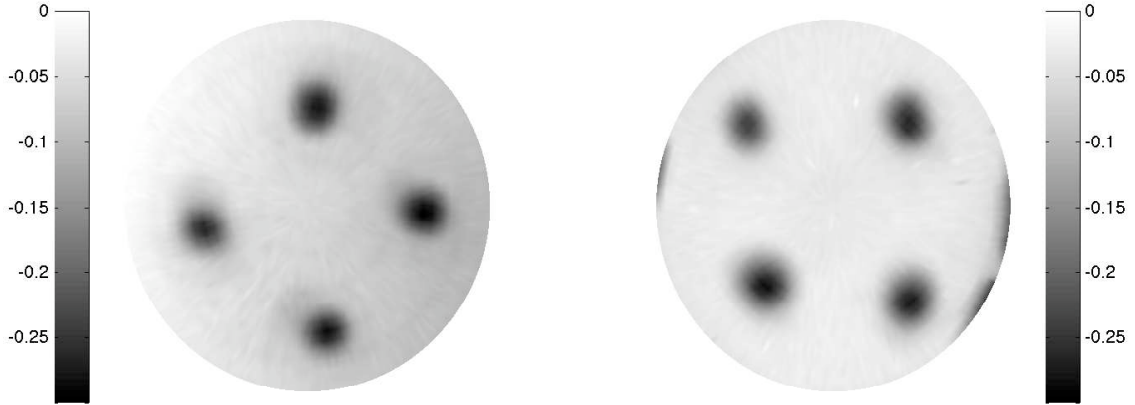


Figure 2. Measurements of the flatness of the top (left) and bottom (left) plates. The color scale is in [mm] and negative values correspond to cavities.

2010) but are extended in the present paper. We then machined these bottom and top plates to alter both, their roughness and flatness. The measured roughness of the smooth plates was between $ra = 0.15 \mu\text{m}$ and $ra = 1 \mu\text{m}$ and are planar within $\pm 4 \mu\text{m}$ except for a $15 \mu\text{m}$ bump at one point of the perimeter of the bottom plate.

The alteration of the plates consisted in digging four $250 \mu\text{m}$ deep cavities (figure 2) and sandblasting the surface with glass spheres. The planarity defect has the same characteristic size as the thermal boundary layer thickness $\lambda_\theta \simeq h/2Nu$ at the high Ra of interest ($Ra \sim 2 \cdot 10^{12}$). The sandblasting results in an enhanced roughness of the plate surfaces, which is $ra = (2.95 \pm 0.10) \mu\text{m}$.

The sidewall is made of seamless stainless steel and has thickness of $550 \mu\text{m}$. It has a measured thermal conductance of $163 \mu\text{W/K}$ at 4.7 K . The influence of the sidewall conduction was taken into account using the analytical correction described in (Roche *et al.*, 2001) and verified in (Verzicco, 2002). The impact of the sidewall conduction is negligible at very high Ra . The assembly of the plate-sidewall connection is optimized to prevent “corner” thermal effects, as described in (Gauthier *et al.*, 2007). The measurement protocol is described in (Roche *et al.*, 2010) and its main points are recalled below.

“The top plate is cooled by a helium bath at 4.2 K through a calibrated thermal resistance (several KW^{-1} at 6 K). The temperature is regulated by a PID controller. A constant and distributed Joule heating P is delivered on the bottom plate. The heat leak from the bottom plate to the surroundings has been measured *in situ* in few experiments ($\simeq 200 \text{nW}$ at 4.7 K) and it is three to four decades smaller than the lowest heating applied on the bottom plate to generate convection. This leak is mainly due to the radiative transfer to the environment at 4.2 K . This excellent thermal control is one of the advantages of our cryogenic environment over room temperature convection experiments, along with the excellent thermal properties of the Cu, which provide isothermal plates to the highest heat flux (Verzicco, 2004).

The temperature difference Δ between the plates is measured with an accuracy down to 0.1 mK , thanks to specifically designed thermocouples. For comparison, the smallest Δ in our experiments are about 10 mK . The temperature of each plate is measured with various Ge thermistances. Their calibration is checked *in situ* against the critical temperature T_c of the fluid with a resolution of 0.2 mK . To avoid a common misunderstanding, we stress that all the $Nu(Ra)$ measurements are done far away

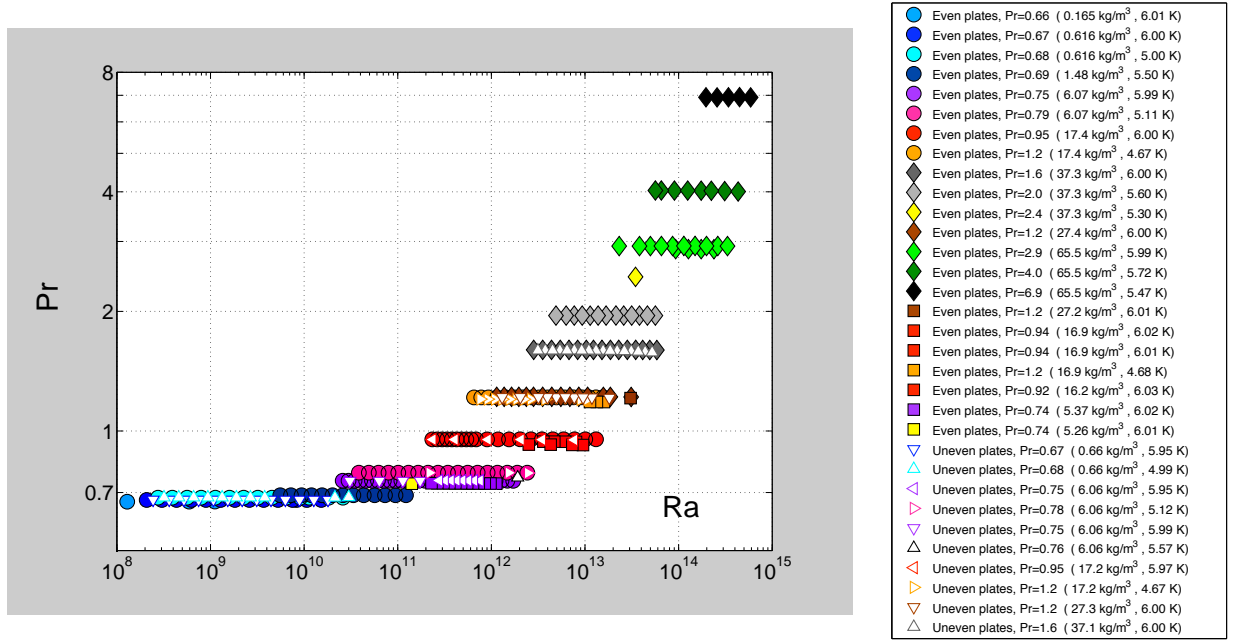


Figure 3. Parameter space of the Pr versus Ra for an elongated cell with even plates (filled symbols) and the same cell after making the plates uneven sand-blasted plates and four cavities on each (open symbols).

from the critical point, as argued in the appendix [of reference (Roche *et al.*, 2010)].

The critical point is simply used here as a thermodynamical reference to cross-check temperature calibration.” [Roche, P.-E.: On the triggering of the Ultimate Regime of Convection, New J. Phys. 12 (2011), p.8]

3. Results and Conclusion

The investigated Pr - Ra parameter space is shown in figure 3 and the heat transfer measurements are plotted in figure 4, using the same symbols. The explanation of the symbols (see figure 3 corresponds to the chronological order of the data acquisition. The measured Nu and the corresponding Ra and Pr are listed in Appendix A for the reference cell and in Appendix B for the altered cell, including the density ρ in kg/m^3 , the mean temperature T in K and the temperature difference between the bottom and the top plates Δ in mK.

A bi-valued Nu is observed with typical 14 % difference between the upper and the lower sets of measurement. Such a bi-stability of heat transfer at high Ra , already reported in a cell with a larger $\Gamma = 0.5$ (Roche *et al.*, 2002), is interpreted as a result of the bi-stability of the large scale circulation in the flow (Roche *et al.*, 2002; Verzicco & Camussi, 2003). But we have to point out that a direct experimental proof of this interpretation is missing. Regardless of the characteristic of the large scale circulation, both the upper and lower subset of Nu experience the transition (defined as a significant change of $Nu(Ra)$ scaling) around $Ra \simeq 2 \cdot 10^{12}$ leading to a scaling $Nu \sim Ra^{0.42}$ on the high Ra side. For each experimental condition, the cell seemed “locked” either on the upper or the lower branch. After the system jumped into the lower branch, it stayed there until the end of the experiment. We note that the lower branch seemed to reconnect smoothly to the upper branch, although further investigations would be need to confirm this point. While an observation of bi-stability could only be seen on the reference cell with smooth and even plates, the transition to the *Ultimate Regime* occurs in both cells, which

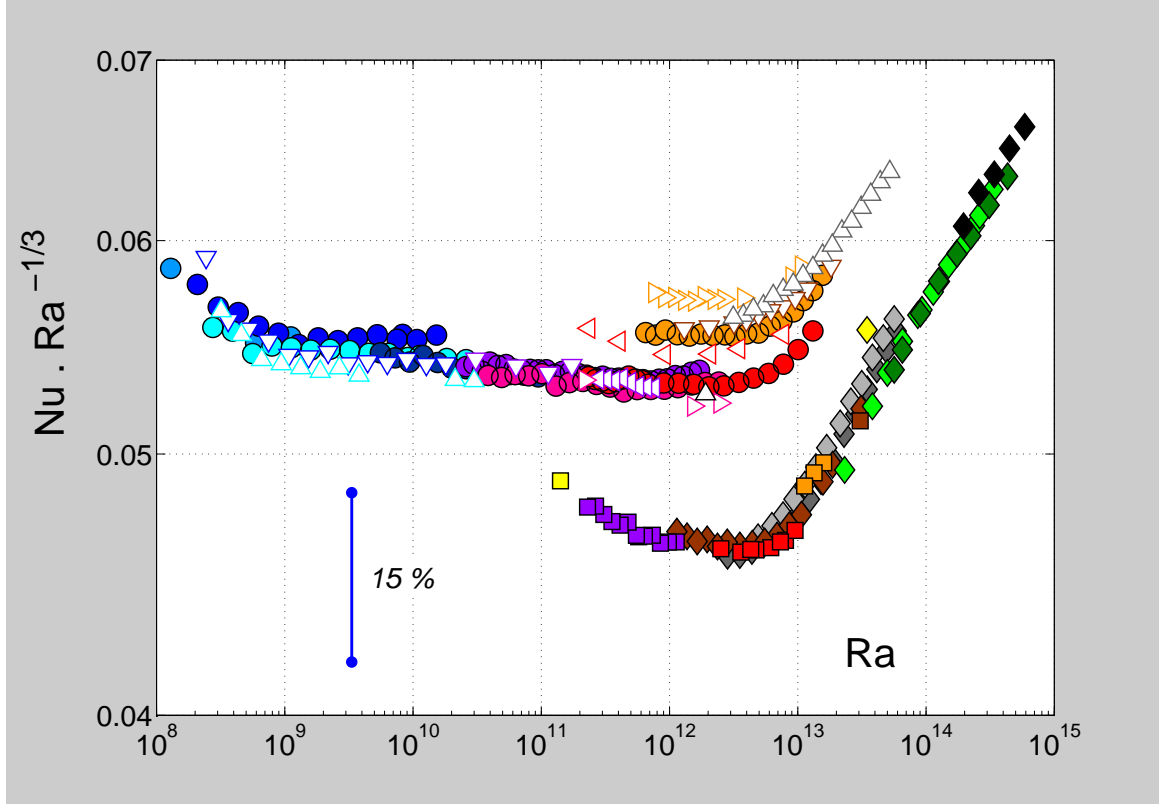


Figure 4. Compensated heat transfer $Nu/Ra^{1/3}$ versus Ra corresponding to the $Ra - Pr$ parameter space shown in figure 3. Filled symbols correspond to the cell with even plates and open symbols to the same cell with uneven plates. The $Nu(Ra)$ -scaling above $Ra \sim 10^{13}$ can be fitted as $Nu \sim Ra^{0.42}$

is the main result of this paper. We cannot exclude that one of the cell is effected by a residual tilt, which might be cause or prevent bi-stability.

As a main conclusion, planeity defects on the plates of Rayleigh-Bénard cell seem to have little impact of the occurrence of a transition to the *Ultimate Regime* of convection, at least when the typical depth of these defects is comparable to the thickness of the thermal boundary layers. Furthermore at a given Pr the $Nu \sim Ra^{1/3}$ -regime is evidenced very clearly in this elongated cell, suggesting that the confinement by the sidewall “breaks” the long range correlation which prevents a interaction between the plates. This suggest that small aspect ratio cells are adequate to investigate the $Nu \sim Ra^{1/3}$ scaling regime.

Acknowledgments

We thank R. du Puits and B. Castaing for interesting discussions and G. Kapoujyan from the SERAS/CNRS for the flatness measurements. Support from the Egide-Procope program and from the DAAD exchange program is acknowledged with pleasure.

References

CHAVANNE, X., CHILLA, F., CASTAING, B., HEBRAL, B., CHABAUD, B. & CHAUSSY, J. 1997

Observation of the ultimate regime in Rayleigh-Benard convection. *Physical Review Letters* **79** (19), 3648–3651.

- GAUTHIER, F., HÉBRAL, B., MUZELLIER, J. & ROCHE, P.-E. 2007 Ultimate regime of convection: search for a hidden triggering parameter. In *Advances in Turbulence XI* (ed. J.M.L.M. Palma & A. Silva Lopes), *Springer Proc. in Physics*, vol. 117, p. 645. Springer (Heidelberg).
- KRAICHNAN, R. 1962 Turbulent thermal convection at arbitrary Prandtl number. *Physics of Fluids* **5** (11), 1374–1389.
- ROCHE, P.-E., CASTAING, B., CHABAUD, B. & HEBRAL, B. 2002 Prandtl and Rayleigh numbers dependences in Rayleigh-Benard convection. *Europhysics Letter* **58** (5), 693–698.
- ROCHE, P.-E., CASTAING, B., CHABAUD, B., HEBRAL, B. & SOMMERIA, J. 2001 Side wall effects in Rayleigh Benard experiments. *European Physical Journal B* **24** (3), 405–408.
- ROCHE, P.-E., GAUTHIER, F., KAISER, R. & SALORT, J. 2010 On the triggering of the Ultimate Regime of convection. *New Journal of Physics* **12**.
- STEVENS, R.J.A.M., LOHSE, D. & VERZICCO, R. 2011 Prandtl and Rayleigh number dependence of heat transport in high Rayleigh number thermal convection. **Submitted to Journal of Fluid Mechanics**.
- VERZICCO, R. 2002 Sidewall finite-conductivity effects in confined turbulent thermal convection. *Journal of Fluid Mechanics* **473**, 201–210.
- VERZICCO, R. 2004 Effects of nonperfect thermal sources in turbulent thermal convection. *Physics of Fluids* **16** (6), 1965–1979.
- VERZICCO, R. & CAMUSSI, R. 2003 Numerical experiments on strongly turbulent thermal convection in a slender cylindrical cell. *Journal of Fluid Mechanics* **477**, 19–49.

Appendix A. Data - Cigar cell with even plates ($\Gamma = 0.23$)

Ra	Nu	Pr	kg/m^3	T [K]	Δ [mK]
1.290×10^8	2.960×10^1	0.66	0.165	6.053	114.9
5.920×10^8	4.616×10^1	0.66	0.165	6.002	512.5
1.115×10^9	5.730×10^1	0.66	0.165	5.973	952.1
8.306×10^9	1.122×10^2	0.67	0.616	5.998	507.2
5.266×10^9	9.632×10^1	0.67	0.616	6.001	322.2
3.702×10^9	8.541×10^1	0.67	0.616	6.001	226.8
2.602×10^9	7.577×10^1	0.67	0.616	6.001	159.7
1.526×10^{10}	1.373×10^2	0.67	0.616	6.003	933.4
1.073×10^{10}	1.216×10^2	0.67	0.616	6.002	656.0
7.527×10^9	1.081×10^2	0.67	0.616	6.001	460.2
6.246×10^8	4.768×10^1	0.67	0.616	6.001	39.0
4.340×10^8	4.272×10^1	0.67	0.616	6.001	27.3
3.026×10^8	3.806×10^1	0.67	0.616	6.001	19.3
2.085×10^8	3.427×10^1	0.67	0.616	6.001	13.5
1.823×10^9	6.746×10^1	0.67	0.616	6.001	112.1
1.284×10^9	5.967×10^1	0.67	0.616	6.001	79.2
8.949×10^8	5.342×10^1	0.67	0.616	6.001	55.4
7.946×10^8	5.079×10^1	0.68	0.616	4.998	30.1
5.629×10^8	4.498×10^1	0.68	0.616	4.999	21.5
3.914×10^8	4.062×10^1	0.68	0.616	4.999	15.2
2.749×10^8	3.622×10^1	0.68	0.616	4.999	10.9
2.597×10^{10}	1.605×10^2	0.68	0.616	4.999	956.5
1.831×10^{10}	1.430×10^2	0.68	0.616	4.997	674.2
3.204×10^9	8.052×10^1	0.68	0.616	4.998	118.7
2.261×10^9	7.177×10^1	0.68	0.616	4.998	84.0
1.598×10^9	6.388×10^1	0.68	0.616	4.998	59.6
1.127×10^9	5.697×10^1	0.68	0.616	4.999	42.3
1.130×10^{10}	1.221×10^2	0.68	0.616	4.997	416.3
9.126×10^9	1.135×10^2	0.68	0.616	4.997	336.3
6.431×10^9	1.013×10^2	0.68	0.616	4.997	237.2
4.542×10^9	9.024×10^1	0.68	0.616	4.997	167.9

1.555×10^{10}	1.349×10^2	0.69	1.48	5.502	126.1
1.199×10^{10}	1.245×10^2	0.69	1.48	5.502	97.4
9.397×10^9	1.141×10^2	0.69	1.48	5.487	76.0
7.238×10^9	1.050×10^2	0.69	1.48	5.494	58.9
5.565×10^9	9.661×10^1	0.69	1.48	5.502	45.7
4.338×10^{10}	1.887×10^2	0.69	1.48	5.503	350.4
3.362×10^{10}	1.732×10^2	0.69	1.48	5.503	271.8
2.600×10^{10}	1.593×10^2	0.69	1.48	5.502	210.3
2.013×10^{10}	1.463×10^2	0.69	1.48	5.502	163.1
9.471×10^{10}	2.434×10^2	0.69	1.48	5.489	758.9
7.317×10^{10}	2.237×10^2	0.69	1.48	5.489	586.3
1.225×10^{11}	2.655×10^2	0.69	1.48	5.488	981.3
5.660×10^{10}	2.054×10^2	0.69	1.48	5.489	453.7
1.714×10^{12}	6.427×10^2	0.75	6.07	5.994	892.7
1.482×10^{12}	6.114×10^2	0.75	6.07	5.992	771.6
1.284×10^{12}	5.808×10^2	0.75	6.07	5.991	668.1
1.109×10^{12}	5.535×10^2	0.75	6.07	5.990	577.0
9.606×10^{11}	5.261×10^2	0.75	6.07	5.990	499.8
8.308×10^{11}	5.011×10^2	0.75	6.07	5.990	432.4
2.255×10^{11}	3.255×10^2	0.75	6.07	5.991	118.1
1.687×10^{11}	2.964×10^2	0.75	6.07	5.991	88.5
1.267×10^{11}	2.688×10^2	0.75	6.07	5.991	66.7
9.474×10^{10}	2.449×10^2	0.75	6.07	5.991	50.1
7.189×10^{11}	4.768×10^2	0.75	6.07	5.990	374.4
6.215×10^{11}	4.547×10^2	0.75	6.07	5.990	323.7
5.376×10^{11}	4.333×10^2	0.75	6.07	5.990	280.1
4.655×10^{11}	4.126×10^2	0.75	6.07	5.990	242.7
4.022×10^{11}	3.938×10^2	0.75	6.07	5.990	209.8
3.482×10^{11}	3.752×10^2	0.75	6.07	5.990	181.8
3.011×10^{11}	3.581×10^2	0.75	6.07	5.990	157.3
2.609×10^{11}	3.410×10^2	0.75	6.07	5.991	136.4
7.106×10^{10}	2.224×10^2	0.75	6.07	5.992	37.8
6.149×10^{10}	2.122×10^2	0.75	6.07	5.991	32.9
5.310×10^{10}	2.029×10^2	0.75	6.07	5.991	28.5
4.600×10^{10}	1.932×10^2	0.75	6.07	5.991	24.8
3.974×10^{10}	1.846×10^2	0.75	6.07	5.991	21.5
3.461×10^{10}	1.749×10^2	0.75	6.07	5.991	18.9
2.982×10^{10}	1.674×10^2	0.75	6.07	5.992	16.4
2.584×10^{10}	1.593×10^2	0.75	6.07	5.992	14.3
1.951×10^{11}	3.106×10^2	0.75	6.07	5.991	102.3
1.460×10^{11}	2.826×10^2	0.75	6.07	5.991	76.8
1.094×10^{11}	2.570×10^2	0.75	6.07	5.991	57.7
8.201×10^{10}	2.335×10^2	0.75	6.07	5.991	43.5
3.441×10^{11}	3.710×10^2	0.79	6.07	5.107	111.1
2.695×10^{11}	3.427×10^2	0.79	6.07	5.107	87.2
2.110×10^{11}	3.167×10^2	0.79	6.07	5.107	68.5
1.657×10^{11}	2.919×10^2	0.79	6.07	5.108	54.0
1.303×10^{11}	2.686×10^2	0.79	6.07	5.108	42.7
1.164×10^{12}	5.566×10^2	0.79	6.07	5.105	373.6
9.124×10^{11}	5.125×10^2	0.79	6.07	5.106	293.0
7.150×10^{11}	4.724×10^2	0.79	6.07	5.106	229.8
5.605×10^{11}	4.356×10^2	0.79	6.07	5.106	180.4
4.401×10^{11}	4.010×10^2	0.79	6.07	5.106	141.9
1.014×10^{11}	2.497×10^2	0.79	6.07	5.108	33.4
7.970×10^{10}	2.300×10^2	0.79	6.07	5.108	26.5
6.248×10^{10}	2.123×10^2	0.79	6.07	5.108	20.9
4.909×10^{10}	1.954×10^2	0.79	6.07	5.108	16.7
3.845×10^{10}	1.805×10^2	0.79	6.07	5.108	13.2
1.896×10^{12}	6.578×10^2	0.79	6.07	5.106	607.9
1.485×10^{12}	6.051×10^2	0.79	6.07	5.106	476.2
2.424×10^{12}	7.142×10^2	0.79	6.07	5.108	778.0
2.652×10^{12}	7.335×10^2	0.95	17.4	6.002	109.6
1.545×10^{12}	6.135×10^2	0.95	17.4	6.003	64.4
9.014×10^{11}	5.132×10^2	0.95	17.4	6.005	38.0
1.180×10^{12}	5.613×10^2	0.95	17.4	6.004	49.4
2.026×10^{12}	6.701×10^2	0.95	17.4	6.003	84.0
7.741×10^{12}	1.068×10^3	0.95	17.4	6.001	317.7
4.533×10^{12}	8.829×10^2	0.95	17.4	6.001	186.5
3.467×10^{12}	8.045×10^2	0.95	17.4	6.002	142.9
5.930×10^{12}	9.695×10^2	0.95	17.4	6.001	243.6
6.894×10^{11}	4.688×10^2	0.95	17.4	6.005	29.3
5.412×10^{11}	4.344×10^2	0.95	17.4	6.006	23.3
4.262×10^{11}	4.011×10^2	0.95	17.4	6.006	18.5

3.365×10^{11}	3.693×10^2	0.95	17.4	6.006	14.9
2.643×10^{11}	3.420×10^2	0.95	17.4	6.006	11.9
2.341×10^{11}	3.292×10^2	0.95	17.4	6.006	10.7
2.982×10^{11}	3.555×10^2	0.95	17.4	6.006	13.3
3.788×10^{11}	3.848×10^2	0.95	17.4	6.006	16.6
4.794×10^{11}	4.183×10^2	0.95	17.4	6.005	20.7
6.104×10^{11}	4.517×10^2	0.95	17.4	6.005	26.1
1.009×10^{13}	1.181×10^3	0.95	17.4	6.001	413.7
1.312×10^{13}	1.310×10^3	0.95	17.4	6.003	538.2
7.800×10^{11}	5.095×10^2	1.21	17.4	4.668	12.1
6.520×10^{11}	4.810×10^2	1.21	17.4	4.668	10.3
9.272×10^{12}	1.186×10^3	1.22	17.4	4.668	130.4
6.093×10^{12}	1.019×10^3	1.21	17.4	4.668	86.1
3.993×10^{12}	8.789×10^2	1.21	17.4	4.668	56.9
3.232×10^{12}	8.172×10^2	1.21	17.4	4.668	46.2
4.941×10^{12}	9.444×10^2	1.21	17.4	4.668	70.1
7.526×10^{12}	1.097×10^3	1.22	17.4	4.668	106.1
2.702×10^{12}	7.710×10^2	1.21	17.4	4.669	38.9
1.764×10^{12}	6.693×10^2	1.21	17.4	4.668	25.8
1.152×10^{12}	5.804×10^2	1.21	17.4	4.668	17.3
9.287×10^{11}	5.423×10^2	1.21	17.4	4.668	14.1
1.427×10^{12}	6.226×10^2	1.21	17.4	4.668	21.1
2.185×10^{12}	7.179×10^2	1.22	17.4	4.668	31.6
1.556×10^{13}	1.454×10^3	1.22	17.4	4.666	217.5
1.102×10^{13}	1.268×10^3	1.22	17.4	4.667	154.7
1.311×10^{13}	1.355×10^3	1.22	17.4	4.667	183.7
3.482×10^{13}	1.725×10^3	1.60	37.3	6.001	119.6
2.297×10^{13}	1.446×10^3	1.60	37.3	6.001	79.3
1.520×10^{13}	1.210×10^3	1.60	37.3	6.001	52.9
1.233×10^{13}	1.111×10^3	1.60	37.3	6.000	43.2
1.871×10^{13}	1.321×10^3	1.60	37.3	6.000	64.8
2.832×10^{13}	1.577×10^3	1.60	37.3	6.001	97.5
4.927×10^{13}	2.004×10^3	1.60	37.3	6.002	168.8
4.141×10^{13}	1.859×10^3	1.60	37.3	6.001	142.0
5.866×10^{13}	2.158×10^3	1.60	37.3	6.003	201.0
1.035×10^{13}	1.037×10^3	1.60	37.3	6.000	36.4
6.754×10^{12}	8.819×10^2	1.60	37.3	6.000	24.2
4.392×10^{12}	7.538×10^2	1.60	37.3	6.000	16.2
3.533×10^{12}	6.986×10^2	1.60	37.3	6.000	13.3
5.450×10^{12}	8.147×10^2	1.60	37.3	6.000	19.8
8.365×10^{12}	9.555×10^2	1.60	37.3	6.000	29.7
2.836×10^{12}	6.489×10^2	1.60	37.3	6.000	10.9
5.653×10^{13}	2.153×10^3	1.95	37.3	5.597	109.6
3.821×10^{13}	1.829×10^3	1.95	37.3	5.597	74.5
2.596×10^{13}	1.549×10^3	1.95	37.3	5.597	51.1
2.142×10^{13}	1.425×10^3	1.95	37.3	5.596	42.4
3.157×10^{13}	1.678×10^3	1.95	37.3	5.597	61.8
4.645×10^{13}	1.984×10^3	1.95	37.3	5.597	90.3
1.679×10^{13}	1.287×10^3	1.95	37.3	5.597	33.5
1.137×10^{13}	1.095×10^3	1.95	37.3	5.598	23.2
7.684×10^{12}	9.364×10^2	1.95	37.3	5.597	16.1
6.298×10^{12}	8.683×10^2	1.95	37.3	5.597	13.5
9.345×10^{12}	1.013×10^3	1.95	37.3	5.597	19.3
1.383×10^{13}	1.187×10^3	1.95	37.3	5.597	27.9
4.904×10^{12}	7.912×10^2	1.95	37.3	5.597	10.8
3.472×10^{13}	1.814×10^3	2.44	37.3	5.302	38.4
1.069×10^{13}	1.046×10^3	1.22	27.4	6.000	112.8
6.900×10^{12}	8.878×10^2	1.22	27.4	6.000	73.2
4.425×10^{12}	7.604×10^2	1.22	27.4	5.999	47.4
3.539×10^{12}	7.047×10^2	1.22	27.4	5.999	38.1
5.533×10^{12}	8.206×10^2	1.22	27.4	5.999	58.9
8.589×10^{12}	9.634×10^2	1.22	27.4	5.999	90.9
3.112×10^{13}	1.635×10^3	1.22	27.4	6.004	327.4
1.573×10^{13}	1.224×10^3	1.22	27.4	6.001	165.5
1.866×10^{13}	1.314×10^3	1.22	27.4	6.001	196.2
2.821×10^{12}	6.551×10^2	1.22	27.4	5.999	30.6
1.966×10^{12}	5.823×10^2	1.22	27.4	6.000	21.7
1.370×10^{12}	5.177×10^2	1.22	27.4	6.000	15.5
1.142×10^{12}	4.890×10^2	1.22	27.4	6.000	13.1
1.645×10^{12}	5.478×10^2	1.22	27.4	6.000	18.4
2.363×10^{12}	6.154×10^2	1.22	27.4	6.000	25.9
2.388×10^{14}	3.770×10^3	2.87	65.5	5.999	104.9
1.273×10^{14}	2.915×10^3	2.87	65.5	5.998	56.5
9.314×10^{13}	2.564×10^3	2.87	65.5	5.998	41.7

Ra	Nu	Pr	ρ [kg/m ³]	T [K]	Δ [mK]
7.477×10^8	4.999×10^1	0.67	0.66	5.946	39.5
5.203×10^8	4.475×10^1	0.67	0.66	5.945	27.8
3.623×10^8	3.996×10^1	0.67	0.66	5.945	19.6
2.437×10^8	3.695×10^1	0.67	0.66	5.944	13.4
6.310×10^9	9.984×10^1	0.67	0.66	5.956	329.2
4.435×10^9	8.890×10^1	0.67	0.66	5.952	231.2
3.122×10^9	7.895×10^1	0.67	0.66	5.950	162.8
2.178×10^9	7.070×10^1	0.67	0.66	5.948	113.8
1.534×10^9	6.266×10^1	0.67	0.66	5.947	80.3
1.075×10^9	5.574×10^1	0.67	0.66	5.946	56.5
1.800×10^{10}	1.416×10^2	0.67	0.66	5.981	948.3
1.272×10^{10}	1.260×10^2	0.67	0.66	5.970	666.5
8.940×10^9	1.125×10^2	0.67	0.66	5.961	467.1
9.395×10^8	5.289×10^1	0.68	0.66	4.980	30.6
6.611×10^8	4.721×10^1	0.68	0.66	4.980	21.8

Appendix B. Data - Cigar cell with uneven plates ($\Gamma = 0.23$)

Ra	Nu	Pr	ρ [kg/m ³]	T [K]	Δ [mK]
7.477×10^8	4.999×10^1	0.67	0.66	5.946	39.5
5.203×10^8	4.475×10^1	0.67	0.66	5.945	27.8
3.623×10^8	3.996×10^1	0.67	0.66	5.945	19.6
2.437×10^8	3.695×10^1	0.67	0.66	5.944	13.4
6.310×10^9	9.984×10^1	0.67	0.66	5.956	329.2
4.435×10^9	8.890×10^1	0.67	0.66	5.952	231.2
3.122×10^9	7.895×10^1	0.67	0.66	5.950	162.8
2.178×10^9	7.070×10^1	0.67	0.66	5.948	113.8
1.534×10^9	6.266×10^1	0.67	0.66	5.947	80.3
1.075×10^9	5.574×10^1	0.67	0.66	5.946	56.5
1.800×10^{10}	1.416×10^2	0.67	0.66	5.981	948.3
1.272×10^{10}	1.260×10^2	0.67	0.66	5.970	666.5
8.940×10^9	1.125×10^2	0.67	0.66	5.961	467.1
9.395×10^8	5.289×10^1	0.68	0.66	4.980	30.6
6.611×10^8	4.721×10^1	0.68	0.66	4.980	21.8

4.591×10^8	4.271×10^1	0.68	0.66	4.980	15.4
3.186×10^8	3.859×10^1	0.68	0.66	4.980	10.9
3.794×10^9	8.341×10^1	0.68	0.66	4.983	121.1
2.671×10^9	7.466×10^1	0.68	0.66	4.982	85.5
1.892×10^9	6.635×10^1	0.68	0.66	4.981	60.8
1.333×10^9	5.923×10^1	0.68	0.66	4.981	43.1
2.132×10^{10}	1.477×10^2	0.68	0.66	4.999	683.3
2.996×10^{10}	1.653×10^2	0.68	0.66	5.008	967.3
7.532×10^{11}	4.814×10^2	0.75	6.06	5.959	387.7
6.534×10^{11}	4.594×10^2	0.75	6.06	5.955	335.8
5.666×10^{11}	4.384×10^2	0.75	6.06	5.952	290.9
4.903×10^{11}	4.192×10^2	0.75	6.06	5.949	251.5
4.241×10^{11}	4.007×10^2	0.75	6.06	5.946	217.4
3.683×10^{11}	3.815×10^2	0.75	6.06	5.945	188.7
3.190×10^{11}	3.642×10^2	0.75	6.06	5.943	163.5
2.766×10^{11}	3.473×10^2	0.75	6.06	5.942	141.8
2.464×10^{12}	7.053×10^2	0.78	6.06	5.128	803.9
1.535×10^{12}	6.008×10^2	0.78	6.06	5.112	496.2
2.188×10^{11}	3.209×10^2	0.78	6.06	5.106	71.3
1.737×10^{11}	3.010×10^2	0.75	6.06	5.995	91.7
1.135×10^{11}	2.594×10^2	0.75	6.06	5.995	60.2
6.357×10^{10}	2.152×10^2	0.75	6.06	5.994	34.1
3.080×10^{10}	1.700×10^2	0.75	6.06	5.994	17.0
1.911×10^{12}	6.531×10^2	0.76	6.06	5.573	805.2
7.645×10^{12}	1.091×10^3	0.95	17.2	5.982	322.2
3.476×10^{12}	8.288×10^2	0.95	17.2	5.969	145.9
2.060×10^{12}	6.930×10^2	0.95	17.2	5.968	86.8
9.155×10^{11}	5.286×10^2	0.95	17.2	5.966	39.1
4.061×10^{11}	4.077×10^2	0.95	17.2	5.966	17.9
2.354×10^{11}	3.437×10^2	0.95	17.2	5.966	10.8
8.987×10^{12}	1.209×10^3	1.20	17.2	4.675	133.7
3.772×10^{12}	8.893×10^2	1.20	17.2	4.671	56.5
1.063×10^{13}	1.291×10^3	1.20	17.2	4.678	158.3
2.652×10^{12}	7.897×10^2	1.20	17.2	4.670	40.0
2.222×10^{12}	7.445×10^2	1.20	17.2	4.669	33.7
1.858×10^{12}	7.032×10^2	1.20	17.2	4.669	28.4
1.561×10^{12}	6.609×10^2	1.20	17.2	4.669	24.0
1.307×10^{12}	6.234×10^2	1.20	17.2	4.669	20.3
1.093×10^{12}	5.887×10^2	1.20	17.2	4.668	17.2
9.154×10^{11}	5.549×10^2	1.20	17.2	4.668	14.6
7.639×10^{11}	5.246×10^2	1.20	17.2	4.668	12.4
1.185×10^{13}	1.313×10^3	1.21	27.3	6.002	127.0
7.688×10^{12}	1.119×10^3	1.22	27.3	5.996	82.4
4.951×10^{12}	9.596×10^2	1.22	27.3	5.994	53.4
3.973×10^{12}	8.878×10^2	1.22	27.3	5.993	43.0
6.171×10^{12}	1.037×10^3	1.22	27.3	5.994	66.3
9.557×10^{12}	1.212×10^3	1.22	27.3	5.998	102.3
3.183×10^{12}	8.227×10^2	1.22	27.3	5.992	34.7
2.039×10^{12}	7.069×10^2	1.22	27.3	5.992	22.7
1.305×10^{12}	6.081×10^2	1.22	27.3	5.992	14.9
1.818×10^{13}	1.544×10^3	1.21	27.3	6.010	195.4
4.395×10^{13}	2.226×10^3	1.58	37.1	6.018	156.8
3.125×10^{13}	1.944×10^3	1.59	37.1	6.009	110.6
2.211×10^{13}	1.698×10^3	1.59	37.1	6.003	78.1
1.561×10^{13}	1.481×10^3	1.59	37.1	6.000	55.4
1.312×10^{13}	1.383×10^3	1.59	37.1	5.999	46.7
1.861×10^{13}	1.583×10^3	1.59	37.1	6.001	65.8
2.633×10^{13}	1.814×10^3	1.59	37.1	6.005	93.1
3.709×10^{13}	2.081×10^3	1.58	37.1	6.012	131.6
5.217×10^{13}	2.378×10^3	1.58	37.1	6.024	187.2
1.100×10^{13}	1.295×10^3	1.59	37.1	5.998	39.3
7.703×10^{12}	1.136×10^3	1.59	37.1	5.996	27.9
5.399×10^{12}	9.954×10^2	1.59	37.1	5.996	19.9
3.768×10^{12}	8.758×10^2	1.59	37.1	5.995	14.3
3.141×10^{12}	8.229×10^2	1.59	37.1	5.995	12.1
4.506×10^{12}	9.346×10^2	1.59	37.1	5.996	16.8
6.442×10^{12}	1.065×10^3	1.59	37.1	5.996	23.5
9.216×10^{12}	1.212×10^3	1.59	37.1	5.997	33.1